Endomembrane mutiny: how picornaviruses hijack host organelles to support their replication

Melia, C.E.

CHAPTER 2

ILLUMINATING THE SITES OF ENTEROVIRUS REPLICATION IN LIVING CELLS BY USING A SPLIT-GFP-TAGGED VIRAL PROTEIN

H.M. van der Schaar[1,$], C.E. Melia[2,$], J.A.C. van Bruggen[1,*], J.R.P.M. Strating[1], M.E.D. van Geenen[1], A.J. Koster[2], M. Bárcena[2,&] and F.J.M. van Kuppeveld[1,&]

Published in mSphere 2016. 1(4):e00104-16
DOI: 10.1128/mSphere.00104-16

[1] Department of Infectious Diseases & Immunology, Virology Division, Faculty of Veterinary Medicine, Utrecht University, Utrecht, The Netherlands

[2] Department of Molecular Cell Biology, Section Electron Microscopy, Leiden University Medical Center, Leiden, The Netherlands

*Current address: Department of Hematology, Lymphoma and Myeloma Center, Academic Medical Center Amsterdam, University of Amsterdam, Amsterdam, The Netherlands

[$,&]These authors contributed equally

SUMMARY

Like all other positive-strand RNA viruses, enteroviruses generate new organelles ("replication organelles", ROs) with a unique protein and lipid composition on which they multiply their viral genome. Suitable tools for live-cell imaging of enterovirus ROs are currently unavailable, as recombinant enteroviruses that encode RO-anchored viral proteins tagged with fluorescent reporters have to date not been reported. To overcome this limitation, we used a split-GFP system, comprising a large fragment (S1-10) and a small fragment (S11) of only 16 residues. The GFP(S11) fragment was inserted into the 3A protein of the enterovirus coxsackievirus B3 (CVB3), while the large fragment was supplied by transient or stable expression in cells. The introduction of GFP(S11) did not affect the known functions of 3A when expressed in isolation. Using correlative light electron microscopy (CLEM) we showed that GFP fluorescence was detected at ROs, whose morphologies are essentially identical to those previously observed for wild-type CVB3, indicating that GFP(S11)-tagged 3A proteins assemble with GFP(S1-10) to form GFP for illumination of bona fide ROs. It is well established that enterovirus infection leads to Golgi disintegration. Through live-cell imaging of infected cells expressing an mCherry-tagged Golgi marker, we monitored RO development and revealed the dynamics of Golgi disassembly in real time. Having demonstrated the suitability of this virus for imaging ROs, we constructed a CVB3 encoding GFP(S1-10) and GFP(S11)-tagged 3A to bypass the need to express GFP(S1-10) prior to infection. These tools will have multiple applications in future studies on the origin, location, and function of enterovirus ROs.

INTRODUCTION

The Enterovirus genus of the Picornaviridae family comprises many human pathogens, such as poliovirus, coxsackievirus A and B, enterovirus-68, enterovirus-71, and rhinovirus, which can cause a wide spectrum of illnesses (1). Being obligate intracellular parasites, enteroviruses rely on the machineries of their host cell for propagation. Like all other viruses that carry a positive-sense, single-stranded RNA genome, enteroviruses redecorate the cell's interior to form new membranous structures that serve as a platform for viral RNA replication (2–6). These structures may aid in concentrating as well as in conferring the proper topology of all required components for genome replication. Furthermore, it has been suggested that they can shield viral RNA products from degradation by cellular RNAses or from detection by sensors of the innate immune system (7, 8).

The morphology of the enterovirus-induced membrane structures (often termed "replication organelles", ROs) has been a subject of intense investigation. Two-dimensional electron microscopy (EM) studies have shown both single-membrane and double-membrane structures, depending on the cell type, time point, and experimental procedure (9–16). Recently, two studies with poliovirus and coxsackievirus B3 (CVB3) were conducted to reveal the three-dimensional structure of the ROs in the course of infection using electron tomography (17, 18). Both studies showed that the first structures detected upon infection are single-membrane tubular structures. These tubules appear to be formed at the expense of Golgi membranes, since the Golgi is in most cell sections no longer detected when the tubules are present. The tubules emerge during the exponential phase of viral RNA replication, suggesting that they are the pre-eminent structures supporting viral genome

synthesis. Later in infection, the tubular ROs morph into double-membrane vesicles (DMVs) and multilamellar structures, a phenomenon that is reminiscent of autophagy. For poliovius it was shown that newly-synthesized viral RNA localizes not only to the tubular structures, but also to the DMVs, implying that the DMVs may also facilitate genome replication (17). In addition, DMVs have been proposed to mediate non-lytic release of progeny virions (19–21).

While EM analyses have provided insight into the structure of the enterovirus ROs, fluorescence microscopy studies have focused on unraveling their origin by investigating the presence of essential host factors or marker proteins on the ROs. These studies have been performed in cells that had been fixed at various time points post-infection, usually at 1 to 2 hour intervals, which gives limited insight into the dynamics of RO formation. ROs are mostly visualized by immunolabeling using antibodies directed against viral proteins that are anchored in the RO membrane, i.e. 2B, 2C, or 3A. With this approach, ROs were shown to colocalize with several proteins involved in ER-to-Golgi transport (22–25) as well as with LC3, a protein involved in the autophagy pathway (11, 13, 19). However, ROs are not mere remnants of the early secretory pathway or constituents of the autophagy pathway. Instead, enteroviruses seem highly selective in hijacking components from these pathways to create completely new organelles with a unique protein and lipid composition optimized for genome replication (reviewed in (5)).

Although we are learning more and more about the morphology and the origin of enterovirus ROs by three-dimensional EM studies and by fluorescence microscopy of fixed cells, it has not been possible thus far to directly visualize ROs in living cells. Live-cell imaging can provide unprecedented insights into the dynamics of biological processes, including RO formation and viral effects on other cellular structures or organelles, and may capture rare or rapid events that may be missed in the analysis of fixed cells. Moreover, observations by immunolabeling of fixed cells may be compromised by artifacts induced during sample preparation, and should be complemented by live-cell imaging (26). To date, enterovirus ROs have only been monitored indirectly in living cells that expressed a fluorescently labeled cellular protein, the Golgi-resident Arf1-RFP, as an RO marker (22). Yet, the use of a cellular protein as a RO marker may complicate investigations examining the transition from Golgi to early enterovirus ROs. A better strategy for direct visualization of ROs in living cells is to label a viral protein involved in their formation. The enterovirus genome can accept coding sequences of foreign proteins (GFP (27, 28), proLC3 (16), Timer (29), and luciferase (27, 30) among others) at the start of the open-reading frame before the capsid coding region. In addition, a poliovirus encoding a viral proteinase (i.e. the 2A protein) tagged with dsRed was generated (31). However, 2A is not a bona fide RO-marker as it does not localize exclusively to ROs. Attempts to generate enteroviruses that encode fluorescently labeled, membrane-anchored viral proteins to illuminate ROs have thus far been futile, most likely because fusion of a fluorescent protein to an RO-anchored viral protein impaired its function or liberation from the polyprotein. The use of small genetically-encoded tags may overcome this limitation, as evidenced by the successful generation of recombinant polioviruses that encode small epitope tags (such as HA, FLAG, and c-myc) in their 3A protein (32) and a recombinant CVB3 encoding an HA-tag in its 2B protein (33).

In this study, we used a split-GFP system (34) to tag the 3A protein of CVB3, a small protein of 89 amino acids with a C-terminal hydrophobic domain that inserts into the RO membranes (35). This split-GFP system is based on superfolder GFP, a variant of GFP that folds better, matures more rapidly, and fluoresces more brightly than GFP (36). Like GFP, superfolder GFP has a beta barrel structure

consisting of eleven beta-strands, which in this system are split into a large fragment (strands 1-10, S1-10) and a small fragment (S11) of only 16 amino acids. Separately, these two fragments are non-fluorescent. Green fluorescence is emitted only when they assemble into superfolder GFP (34). We show that tagging 3A with GFP(S11) does not affect its known functions when 3A is expressed alone. When introduced into the viral genome of CVB3, GFP(S11)-tagged 3A assembled with GFP(S1-10) to illuminate enterovirus ROs as shown by correlative light electron microscopy (CLEM). We illustrate the suitability of CVB3 encoding this split-GFP-tagged 3A for live-cell imaging by monitoring the development of ROs and the disintegration of the Golgi, as visualized using GM130-mCherry, in infected cells in real time. This new tool simplifies the visualization of enterovirus ROs, avoiding immunolabeling of viral proteins in fixed cells, and will have multiple applications in future studies on the origin, location, and function of enterovirus ROs.

RESULTS

3A tagged with GFP(S11) assembles with GFP(S1-10) to yield GFP fluorescence

In order to visualize the enterovirus ROs in living cells, one of the non-structural proteins that is anchored in the membranes of the ROs should be labeled with a fluorescent tag. A transposon-based insertion mutagenesis study revealed that the N-terminal region of poliovirus 3A tolerates small insertions (32, 37). Specifically, viable insertions were found after residues 2, 6, 9, 10, or 11. Since the 3A proteins of coxsackievirus B3 (CVB3) and poliovirus are highly homologous, these positions were good candidates for introduction of a small tag in CVB3 3A. We chose to insert GFP(S11) after amino acid 2 in CVB3 3A without using any linker residues, yielding 3A(S11aa2) (Fig. 1A).

Before introducing GFP(S11) into the viral genome, we first tested whether inserting the tag into 3A at this position would generate GFP fluorescence upon co-expression with GFP(S1-10). Staining with an anti-3A antibody demonstrated that the expression pattern of 3A(S11aa2) resembled that of untagged 3A (i.e. lacking GFP(S11)) in HeLa (Fig. S1A) and in BGM cells (data not shown), indicating that the GFP(S11)-tag does not alter the localization of 3A. Co-expression of GFP(S1-10) with 3A(S11aa2), but not with untagged 3A, resulted in a GFP signal that greatly overlapped with the 3A-pattern generated with the anti-3A antibody (Fig. S1B, HeLa cells not shown). Furthermore, 3A(S11aa2) was not GFP fluorescent in the absence of GFP(S1-10) (Fig. S1A). Thus, GFP(S1-10) can assemble with 3A(S11aa2) to yield GFP fluorescence at the sites where 3A is localized in the cell.

Introduction of GFP(S11) into 3A does not impair its known functions

Next, we investigated whether 3A(S11aa2) is able to perform the same functions as untagged 3A. Enteroviruses hijack the Golgi-resident PI4KB (phosphatidylinositol 4-kinase III beta) via their 3A protein to ROs to enrich these membranes in PI4P (phosphatidylinositol 4-phosphate), an essential lipid for viral RNA replication (22). In line with previous observations (22, 38, 39), PI4KB was present in a faint Golgi-like pattern in untransfected HeLa cells, whereas in 3A-transfected cells an intese PI4KB signal was detected at membranes containing untagged 3A (Fig. 1B). Likewise, in cells co-expressing 3A(S11aa2) and GFP(S1-10), PI4KB recruitment was observed to the membranes containing fluorescent 3A (Fig. 1B).

The enterovirus 3A protein interacts directly with GBF1, an essential host factor for enterovirus replication (27, 30). Under normal conditions, GBF1 is an activator of the small GTPase Arf1, which

in turn recruits the COP-I complex to Golgi membranes upon activation (40). The COP-I coat initiates budding of transport vesicles that ferry cargo at the ER-Golgi interface and in the Golgi (41). Expression of 3A in isolation leads to the perturbation of ER to Golgi transport (30, 42–44), as

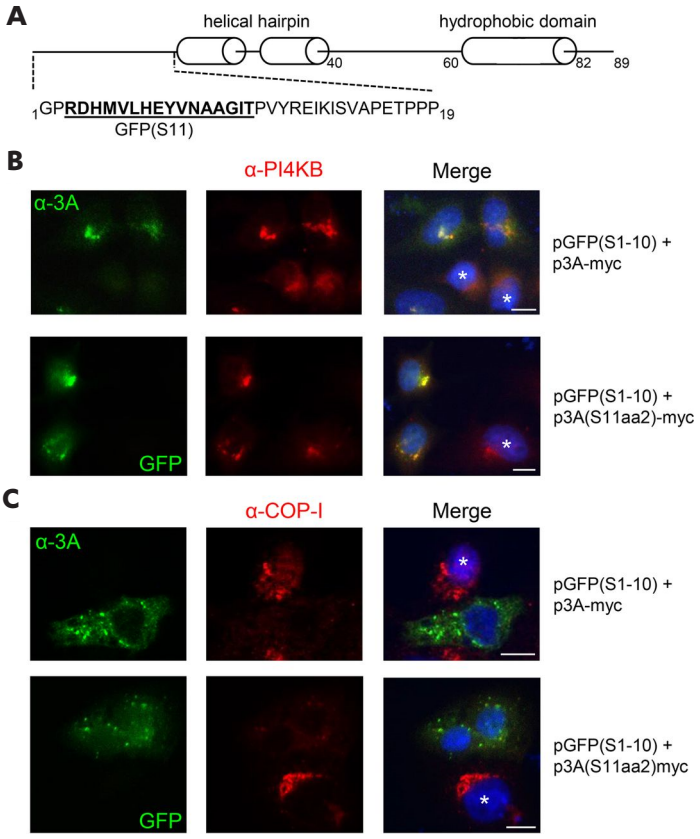

Figure 1. 3A(S11aa2) recruits PI4KB and dissociates COP-I from Golgi membranes. A) The CVB3-3A(S11aa2) protein. The GFP(S11)-tag (bold, underlined) is inserted after amino 2 of 3A without any linker residues. The hydrophobic domain, predicted by the Kyte and Doolittle method (67), is indicated as well as the location of the helical hairpin predicted by NMR analysis of the truncated poliovirus 3A protein (68). B, C) HeLa R19 (B) or BGM (C) cells were co-transfected with the plasmid encoding GFP(S1-10) (i.e. pGFP(S1-10)) and either p3A-myc or p3A(S11aa2)-myc. The next day, cells were fixed and subjected to immunofluorescence analysis. The 3A protein was visualized with an antibody staining for p3A-myc (a primary anti-3A antibody and a secondary Alexa488-labeled antibody), while p3A(S11aa2) was visualized by the GFP fluorescence as a result of assembly with GFP(S1-10). PI4KB (A) or COP-I (B) were detected with immunofluorescence using a secondary Alexa594-labeled antibody. Untransfected cells are indicated with an asterisk. Nuclei were stained with DAPI. Wide-field images were acquired with an Olympus BX60 fluorescence microscope. Scale bars equal 10 µm.

demonstrated by the dissociation of COP-I from Golgi membranes in BGM cells (44), presumably as a result of the interaction of 3A with GBF1 (30, 44). Similar to untagged 3A, 3A(S11aa2) visualized by co-expression of GFP(S1-10) clearly caused COP-I dissociation (Fig. 1C).

In addition to the interaction with GBF1, enterovirus 3A also directly binds to the host factor ACBD3 (acyl-CoA-binding protein domain 3), although the role of this protein in enterovirus

replication is still enigmatic (38, 39, 45–47). We tested whether 3A(S11aa2) could still interact with GBF1 and ACBD3 in a mammalian two-hybrid system (38, 39). Similar to untagged 3A, 3A(S11aa2) interacted with GBF1 and ACBD3, even in the presence of overexpressed GFP(S1-10) (Fig. S2). Collectively, our results demonstrate that introduction of GFP(S11) in CVB3 3A after the second residue does not affect the ability of 3A to interact with previously identified host factors or to perform its known functions, which prompted us to introduce GFP(S11) into the viral genome of CVB3.

Tagging 3A with GFP(S11) results in a replication-competent CVB3 that generates fluorescent replication organelles

Introduction of the GFP(S11)-tag into the infectious clone of CVB3 yielded viable virus, i.e. CVB3-3A(S11aa2). Sequence analysis of the viral genome confirmed that the tag was retained in the 3A protein without mutations. In addition, we generated a replication-competent CVB3 with the short affinity tag StrepII of 10 residues in 3A (i.e. CVB3-3A(StrepIIaa2)). Insertion of the StrepII-tag also did not affect the known functions of 3A (data not shown), and the tag was retained in 3A for five passages (data not shown), further demonstrating that residue 2 is an amenable site for introduction of a small tag.

Subsequently, we tested whether the GFP(S11)-tag in 3A affects the replication kinetics of the virus. Since cells that have been transfected with plasmid DNA are less susceptible to picornavirus infection (48), we generated single cell clones of HeLa and BGM cells that stably express GFP(S1-10). Next, we compared the growth kinetics of CVB3-3A(S11aa2) to wild-type (wt) CVB3 in the presence and in the absence of GFP(S1-10). Samples were subjected to endpoint titration to determine the production of infectious virus, or quantitative PCR to measure viral RNA levels. Replication of wt CVB3 in BGM cells and BGM(GFPS1-10) cells was nearly identical, showing that the presence of GFP(S1-10) did not alter CVB3 replication kinetics (Fig. 2A, 2B). The replication kinetics of tagged CVB3 in BGM(GFPS1-10) also resembled that of BGM cells, indicating that binding of GFP(S1-10) to 3A(S11aa2) does not impede replication (Fig. 2A, 2B). Both infectious virus production and viral RNA levels of the tagged CVB3 were delayed compared to wt CVB3 (Fig. 2B). This delay in replication has also been observed for recombinant polioviruses that encode 3A proteins with small epitope tags (32). Together, these findings showed that replication of CVB3-3A(S11aa2) is similar to other enteroviruses that encoding small tags in a viral protein.

Having produced replication-competent CVB3-3A(S11aa2), we then tested whether this virus induced GFP fluorescence in cells expressing GFP(S1-10). Figure 3 (left images) shows that these cells do emit GFP fluorescence upon infection with CVB3-3A(S11aa2). To investigate whether the GFP fluorescence was restricted to the sites where the 3A(S11aa2) proteins are localized in the cell, we first stained cells with an anti-GFP antibody. Figure 3A shows that the anti-GFP antibody recognized GFP(S1-10) as demonstrated by the cytoplasmic staining in uninfected cells, whereas BGM cells lacking GFP(S1-10) were negative (data not shown). In infected cells, GFP fluorescence was not observed throughout the entire cytoplasm, but instead in a pattern that is reminiscent of a 3A staining pattern. This suggests that assembled, fluorescent GFP is only found at sites that contain 3A(S11aa2). Interestingly, while anti-GFP antibody staining in infected cells was detected throughout the cytoplasm, the signal was more intense at regions corresponding to GFP fluorescence. This is likely the result of recruitment of GFP(S1-10) to sites where 3A is localized. Another possibility is that

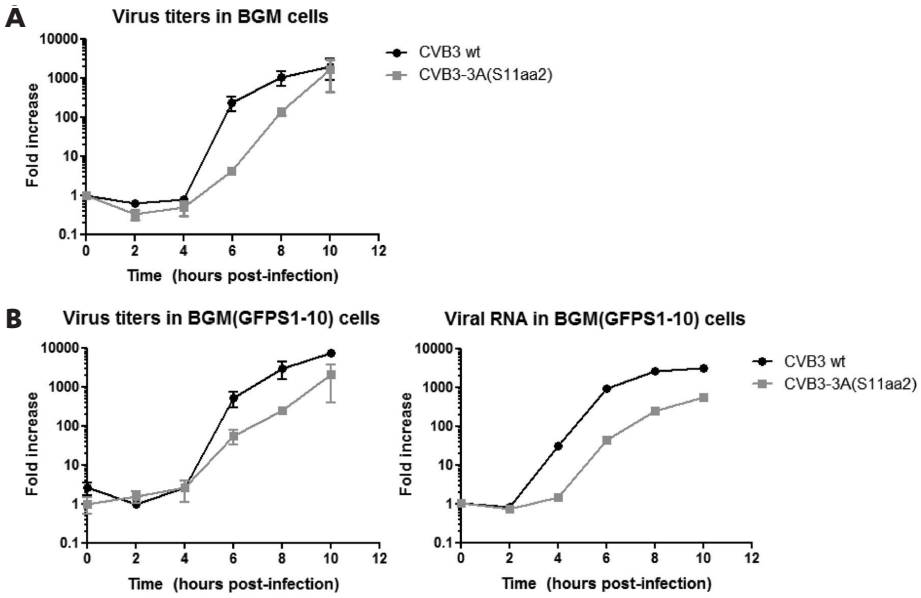

Figure 2. Single-cycle growth curve analysis of CVB3-3A(S11aa2). BGM cells (A) or BGM cells that stably express GFP(S1-10) (B) were infected with wt CVB3 or CVB3-3A(S11aa2) for 30 min at MOI 1. At the indicated time points, cells were subjected to titration analysis after freeze-thawing cycles to determine the amount of infectious virus particles. Alternatively, cells were lysed to determine the amount of viral RNA by quantitative PCR. The results are expressed as fold induction relative to the quantities determined directly after removing the inoculum.

the anti-GFP antibody has a higher affinity for full-length, assembled GFP.

To ensure that GFP fluorescence is exclusively emitted from 3A(S11aa2)-containing sites, cells from the same infection were stained with an anti-3A antibody. Figure 3B shows that GFP fluorescence was detected in a pattern that greatly overlapped with 3A visualized by immunofluorescence. However, the immunofluorescence with the 3A-antibody generated a slightly more extensive 3A-pattern, most likely as a consequence of not all 3A(S11aa2) proteins being bound by GFP(S1-10). This could be due to partial inaccessibility of 3A(S11aa2) proteins to their GFP(S1-10) counterparts as 3A proteins localize to densely-packed ROs.

Next, we set out to confirm that the emerging GFP fluorescence is emitted from ROs that contain 3A(S11aa2). To this end, we applied correlative light electron microscopy (CLEM) (49, 50), which provides a direct link between fluorescent signals and the virus-induced structures that underlie them at high resolution. The emerging fluorescence signal in BGM (GFPS1-10) cells infected with CVB3-3A(S11aa2) and stained with Mitotracker Deep Red FM was monitored by live-cell imaging. Cells were imaged and fixed at an intermediate time point in infection. Following sample processing and EM imaging, the Mitotracker signal and corresponding mitochondria were used to orient fluorescence and EM images with an independent marker. Using this method, 3A(S11aa2) was found to localize to ROs, evident as both tubules and clusters of DMVs and multilamellar structures (Fig. 4). Furthermore, the CLEM results not only show that GFP fluorescence was emitted from bona fide ROs, they also demonstrate that the GFP(S11) insertion in 3A does not affect the development of the different RO morphologies typically observed during enterovirus infections.

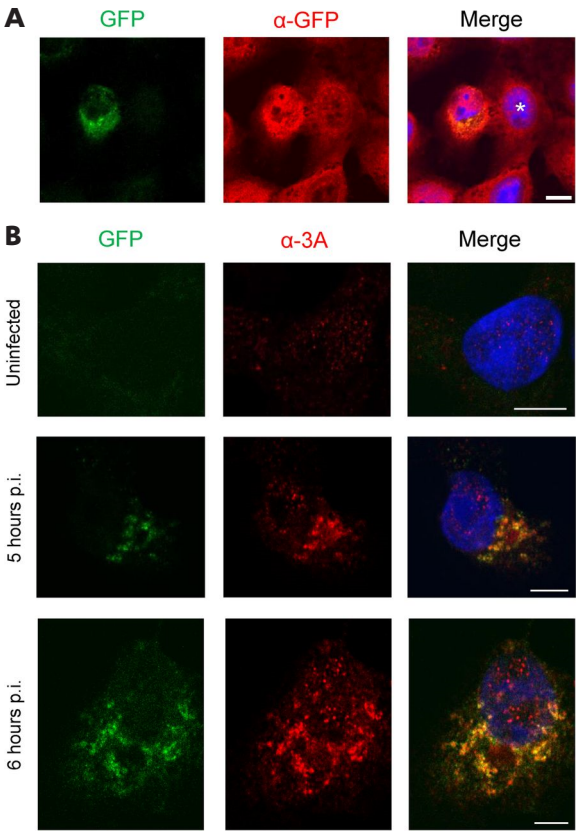

Figure 3. GFP fluorescence is only emitted from sites where 3A(S11aa2) is localized in cells. A, B) BGM cells stably expressing GFP(S1-10) were infected with CVB3-3A(S11aa2). At 5 and 6 h p.i., cells were fixed and subjected to immunofluorescence analysis. The detected GFP fluorescence is the result of GFP(S1-10) assembling with 3A(S11aa2). Nuclei were visualized with DAPI. Images were acquired with a Leica SPE-II DMI-4000 confocal laser scanning microscope. Scale bars equal 10 µm. A) GFP(S1-10) was detected with a primary polyclonal antibody directed against GFP and a secondary Alexa594-labeled antibody. The uninfected cell is marked with an asterisk. B) The 3A(S11aa2) protein was stained with a primary antibody directed against 3A and a secondary Alexa594-labeled antibody. An uninfected cell and typical examples of cells early in infection (5 h p.i.) and later in infection (6 h p.i.) are shown.

Live-cell imaging reveals the dynamics of Golgi disassembly in live infected cells

Enterovirus infections trigger the disassembly of the Golgi apparatus, which coincides with the formation of early ROs (18, 22). Here, we used live-cell imaging to visualize this process in living cells. To this end, BGM cells stably expressing GFP(S1-10) were transduced with MLV particles encoding mCherry-GM130 as a traceable marker for the Golgi. Live-cell confocal imaging was first carried out with a narrow pinhole (95.56 µm) to detect the first local changes in Golgi structure during infection. As expected, GM130 was observed as a condensed perinuclear signal in uninfected cells (Fig. 5A) or early in infection with CVB3-3A(S11aa2) when fluorescent 3A (which will be further referred to as 3A-GFP) could not yet be detected (Fig. 5B, Movies S1 and S2). Strikingly, the first 3A-GFP signal detected in infected cells was rarely associated with GM130, but could instead be observed as distinct cytoplasmic punctae. Localization of 3A-GFP signal to the Golgi region typically occurred

within 25 minutes (n=17, range 0-45 minutes) of initial detection. This was followed by a sharp increase in the intensity and number of Golgi-adjacent 3A-GFP punctae and a local perturbation of Golgi morphology, characterized by the onset of GM130 signal fragmentation (Fig. 5B, asterisk GM130 channel). Interestingly, while this rapidly increasing 3A-GFP signal was clearly detected in the Golgi region, it rarely co-localized directly with the GM130 marker (Fig. 5B inset, arrowhead), which is in agreement with previous observations in fixed cells (22). This suggests that RO membranes originate from a compartment of the Golgi not labeled by the cis-Golgi marker GM130, or that 3A resides there only transiently before accumulating in the ROs.

The first signs of disruption of Golgi morphology largely began during or even preceding the accumulation of visible 3A signal (Fig. 5B asterisk 3A-GFP channel, Movie S1), suggesting that local changes to morphology occur rapidly and may be triggered by 3A accumulation in regions of the Golgi outside the imaging plane. To facilitate the detection of the whole Golgi and to monitor large scale changes in Golgi morphology, imaging was carried out using a wider confocal

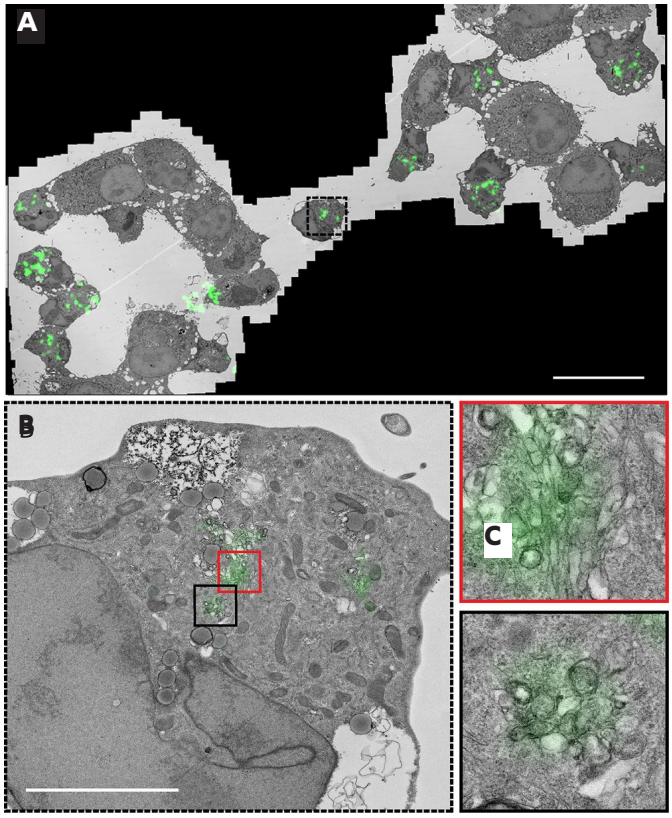

Figure 4. 3A(S11aa2) localizes to ROs that have tubule and DMV morphologies. A, B) BGM GFP(S1-10) cells were infected with CVB3-3A(S11aa2), stained with Mitotracker Deep Red FM and monitored by live cell imaging. Full-depth z-stacks of cells emitting GFP fluorescence were taken and cells were processed for EM. LM-EM overlays were made using the Mitotracker as an orientation guide, and 3A-GFP signal was aligned to the corresponding EM image in this manner first at low magnification (A), and then within individual cells of interest (B, which is the boxed area in A). 3A-GFP signal was found at the typical structures that develop during CVB3 infection, including single-membrane tubules (B, red box, enlargement shown on the right) and double-membrane vesicles (B, black box, enlargement shown on the right). Scale bars equal 30 µm (A) and 5 µm (B).

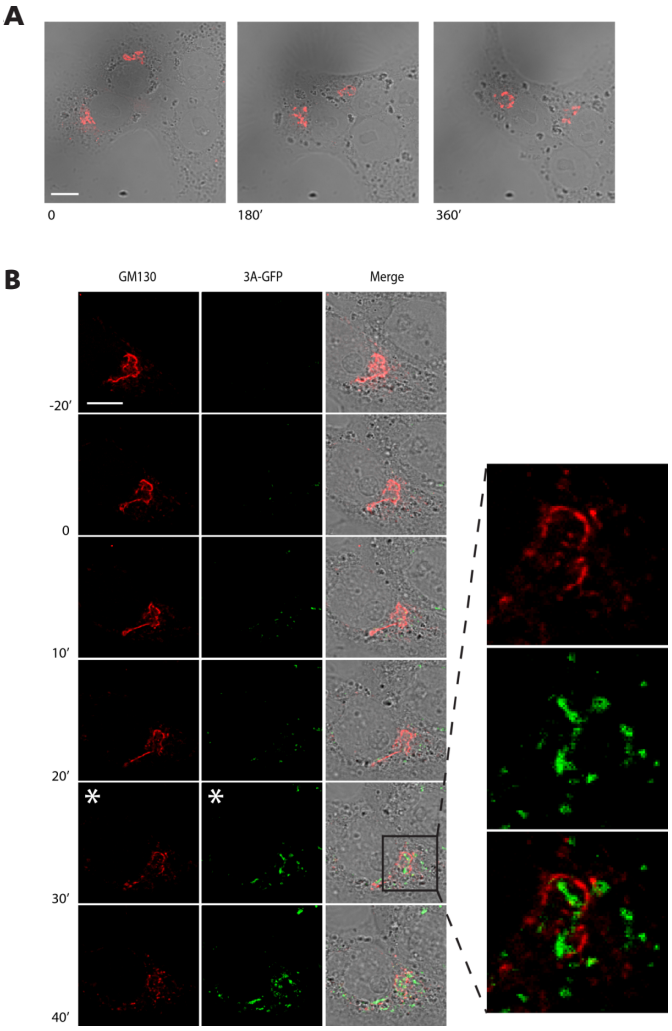

Figure 5. Live-cell imaging reveals the association between 3A accumulation and local perturbation to Golgi morphology. A, B) BGM GFP(S1-10) cells transduced with mCherry-GM130 MLV particles were mock-infected (A) or infected with CVB3-3A(S11aa2) (B), and imaged by live-cell microscopy with images taken at 5 minute intervals. The frames given as time '0' represent either an arbitrary time point (A) or the moment of appearance of 3A-GFP signal (B). Images are presented at 180 (A) or 10 to 20 (B) min intervals as indicated. The confocal pinhole was adjusted for analysis of local effects (95.56 µm confocal pinhole). While Golgi integrity was maintained for the duration of imaging in mock cells (A), local fragmentation of GM130 was evident in infected cells (B, asterisk GM130 channel). The onset of fragmentation was associated with a marked increase in the intensity and number of 3A-GFP punctae at the Golgi (B, asterisk 3A-GFP channel) although, while 3A signal and GM130 were proximal at this stage, there was no clear colocalization (B inset). Scale bar equals 10 µm.

pinhole (600 µm). Global Golgi fragmentation began typically 10-30 minutes after 3A started to accumulate in high amounts (Fig. 6) (n=8, range 0-45 min), which presumably reflects the time taken for the cumulative local changes to become apparent within the entire structure, and was completed 75-105 min after the initial detection of 3A-GFP signal (n=8). Together, these data show that 3A accumulation coincides with the local disruption of Golgi morphology, leading to

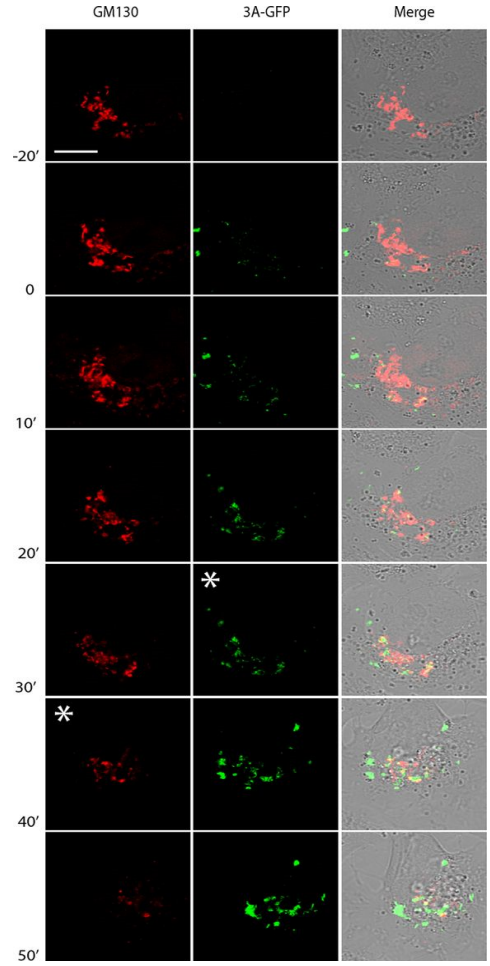

Figure 6. Global disruption to Golgi morphology during CVB3 infection visualized by live-cell imaging. Cells were treated as described in Figure 5. Imaging conditions were adjusted to better ascertain global Golgi morphology (600 µm confocal pinhole) over the course of infection. The frame given as time '0' represents the moment of appearance of 3A-GFP signal. Golgi fragmentation (asterisk GM130 channel) was visible following accumulation of 3A-GFP (asterisk 3A-GFP channel), leading to complete disassembly and a punctate GM130 signal. Scale bar equals 10 µm.

global fragmentation and eventual disassembly of the Golgi apparatus. After complete Golgi fragmentation, the 3A-GFP signal expands throughout the cell and eventually occupies the entire cytoplasm before the cell goes into demise, demonstrating that 3A-GFP signals can be imaged to the point of cell lysis (Movies S1 and S2).

Construction of CVB3 encoding both GFP(S1-10) and 3A(S11aa2)

Studying ROs induced by CVB3 encoding split-GFP-tagged 3A in distinct cell types requires the cellular expression of GFP(S1-10). To bypass the need for delivering the GFP(S1-10) gene via retroviral transduction or by generating stable cell lines, we constructed a CVB3 that encodes not

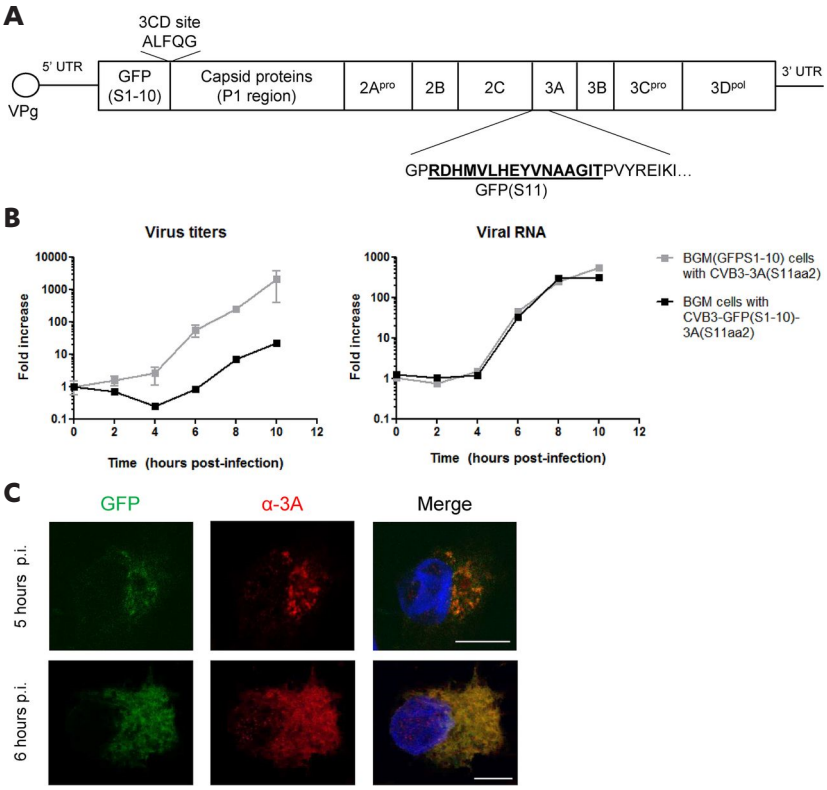

Figure 7. Construction of CVB3 that encodes both GFP(S1-10) and 3A(S11aa2). A) A schematic diagram of the genome organization of CVB3 showing the insertion of GFP(S1-10) before the capsid coding region and GFP(S11) in 3A after amino acid 2. B) Growth curve analysis of CVB3-GFP(S1-10)-3A(S11aa2) in BGM cells and CVB3-3A(S11aa2) in BGM(GFPS1-10) cells. Cells were infected for 30 min at MOI 1. At the indicated time points, cells were subjected to titration analysis after freeze-thawing cycles to determine the amount of infectious virus particles. Alternatively, cells were lysed to determine the amount of viral RNA with quantitative PCR. The results are expressed as fold induction relative to the quantities determined directly after removing the inoculum. C) BGM cells were infected with CVB3 GFP(S1-10) 3A(S11aa2). At 5 and 6 h p.i., cells were fixed and subjected to immunofluorescence analysis. The detected GFP fluorescence resulted from the assembly of GFP(S1-10) with 3A(S11aa2). Nuclei were visualized with DAPI. Images were acquired with a Leica SPE-II DMI-4000 confocal laser scanning microscope. Typical examples of cells early in infection (top panel) and later in infection (lower panel) are shown. Scale bars equal 10 µm.

only 3A(S11aa2) but also GFP(S1-10) (Fig. 7A). For this, the gene encoding GFP(S1-10) was inserted upstream of the capsid coding region (P1) in the infectious clone containing 3A(S11aa2). GFP(S1-10) was followed by an artificial 3CD cleavage site to release the protein from the P1 region upon translation. Viable virus (i.e. CVB3-GFP(S1-10)-3A(S11aa2) was obtained upon transfection of BGM cells with RNA transcripts of the infectious clone. After harvesting CVB3-GFP(S1-10)-3A(S11aa2), we compared its replication kinetics in BGM cells to CVB3-3A(S11aa2) in BGM(GFPS1-10), so that in both cases the 3A(S11aa2) protein would bind to GFP(S1-10). The level of viral RNA replication was nearly identical for both viruses (Fig. 7B), suggesting that the generation of ROs during the course of infection occurs similarly. However, the virus encoding both GFP fragments (i.e. CVB3-GFP(S1-10)-3A(S11aa2)) was delayed in production of infectious progeny in comparison to CVB3-3A(S11aa2) (Fig. 7B). In line with a previous study (51), we found that the processing of the artificial 3CD cleavage site

between a foreign protein and P1 is suboptimal (Fig. S3), which may explain the delay in progeny virion production.

Next, we tested whether BGM cells became GFP fluorescent upon infection with CVB3-GFP(S1-10)-3A(S11aa2). Figure 7C shows that GFP fluorescence colocalized with 3A, visualized with an anti-3A antibody, both early (upper panel) and later (lower panel) in infection. Yet, the GFP fluorescence was substantially dimmer compared to BGM(GFPS1-10) cells infected with CVB3-3A(S11aa2). It is plausible that the dimmer signal is a result of the equimolar ratios of 3A(S11aa2) and GFP(S1-10) generated by this virus, while BGM(GFPS1-10) cells produce an excess of GFP(S1-10). Another explanation for the dim GFP fluorescence is that not all GFP(S1-10) is released from P1 due to suboptimal cleavage of the artificial cleavage site. When GFP(S1-10) is still fused to P1, it might be unable to assemble with 3A(S11aa2) and/or become fluorescent. Nevertheless, these findings suggest that the virus containing both GFP fragments is suitable for live-cell imaging.

DISCUSSION

Live-cell imaging is a powerful technology to gain insight into the dynamics of biological processes. In the field of virology, this method has mostly been applied to visualize the entry and egress pathways of viruses by following the fate of fluorescently labeled, individual virus particles in living cells and monitoring their interactions with cellular structures (52). Imaging replication structures during infection has so far only been reported for a few viruses, including hepatitis C virus (53, 54), vaccinia virus (55), turnip mosaic virus (56), mouse hepatitis virus (57, 58) and equine arteritis virus (59). In most of these studies, replication structures are illuminated by a viral protein that is fused to GFP. Recombinant enteroviruses that encode an RO-anchored viral protein fused to GFP (or another fluorescent reporter) have to date not been reported. Small epitope tags on the other hand were successfully introduced in the 3A protein of poliovirus (32), which prompted us to test whether small tags suitable for fluorescent labeling are accepted in the 3A protein of CVB3. The smallest tag for fluorescent labeling of a protein is the tetracysteine tag of 6-20 residues (depending on the version), but it requires visualization with biarsenical dyes FlAsH and ReAsH in extra labeling steps, and results in fluorescence with a relatively poor quantum yield (60, 61). The split-GFP system uses a tag of 16 residues, GFP(S11), which has the advantage that it does not require staining but becomes directly fluorescent upon assembly with the large GFP(S1-10) fragment in living cells (34). This system has been successfully applied before in the context of a virus to study the intracellular trafficking of ribonucleoproteins of Influenza A virus, where the PB2 polymerase subunit was tagged with GFP(S11) (62). In our study, we incorporated GFP(S11) into the RO-anchored 3A protein of CVB3. We show that the introduction of GFP(S11) after the second residue does not affect the localization or function of 3A when it is expressed in isolation. Whether binding of GFP(S1-10) affects the function of 3A(S11aa2) proteins remains unknown, as it is possible that not all 3A(S11aa2) proteins are bound by the GFP(S1-10) counterparts. Therefore, the subset of unbound 3A(S11aa2) proteins could be solely responsible for exerting the 3A functions.

Having found that the 3A protein was not functionally hampered by the introduction of the GFP(S11)-tag, we generated a recombinant CVB3 that encodes 3A(S11aa2). Infections of this virus in BGM cells stably expressing GFP(S1-10) yielded discrete fluorescent signals. However, confirming that the fluorescent foci localize to virus-induced structures demands the higher resolution images

of sub-cellular structures, in the context of their surroundings, that EM can provide. Establishing this link with ultrastructure is particularly interesting in the case of enteroviruses, since their ROs can adopt various morphologies during infection (i.e. tubules, DMVs, and multilamellar structures) which, as observed by EM, often co-exist. In this study, CLEM was employed to confirm that the GFP fluorescent foci localize to ROs and to establish which subset of enterovirus RO morphologies this fluorescence corresponded to. CLEM revealed that the GFP fluorescence was present at bona fide ROs, which took the form of both tubular structures and DMVs resembling those observed previously with wt CVB3 in Vero cells (18). Split-GFP CLEM thus allows the unambiguous identification of RO morphologies underlying the 3A signal, and opens up new possibilities for a better understanding of the requirements for their development. This method also circumvents limitations inherent in other, similar approaches. For instance, while immuno-gold labeling of proteins is a popular technique that couples an electron-dense gold particle to the protein of interest, allowing it to be visualized by EM, its success depends largely upon the antibody used and the resilience of epitopes during EM sample preparation. In our experience, sample preparation procedures for immunolabeling of CVB3 3A that retain RO membranes unfortunately do so at the expense of viral epitope integrity, resulting in insufficient labeling of 3A (unpublished data).

Enterovirus ROs were imaged in living BGM(GFPS1-10) cells upon infection with CVB3-3A(S11aa2). As a proof of concept, we also expressed GM130-mCherry in these cells to visualize Golgi disassembly in real time. The onset of Golgi fragmentation was found to correspond to a period of rapid 3A accumulation in the Golgi region. Under the experimental conditions used, Golgi disruption was completed within 75-105 min after the first detection of 3A-GFP. Interestingly, while 3A accumulation occurred adjacent to the GM130 signal, 3A rarely co-localized with GM130-mCherry before and during Golgi disassembly. While this does not preclude the transient localization of 3A to the cis-Golgi, our findings suggest that ROs may be generated from another Golgi compartment not labeled by GM130, which is in line with previous observations that suggest that RO formation is initiated at the trans-Golgi (22).

Enteroviruses can infect both polarized and non-polarized cells. The use of CVB3 encoding split-GFP-tagged 3A in distinct cell types relies on the cellular expression of GFP(S1-10). As an alternative to delivering the GFP(S1-10) gene via transduction, we introduced the coding sequence of GFP(S1-10) into the viral genome together with 3A(S11aa2). This new recombinant CVB3 encoding both GFP fragments also induced GFP fluorescent foci that colocalized with 3A. While progeny virion production by this virus was delayed, the viral RNA levels were very similar to CVB3-3A(S11aa2) infection of BGM(GFPS1-10) cells, implying that the "two-fragment virus" retained its ability to form ROs. Hence, this virus would be suitable for studying enterovirus ROs in physiologically more relevant cell types, including pancreatic cells (14) and 3D-cultured CaCo-2 cells (63), without the need for ectopic expression of GFP(S1-10).

In conclusion, we have presented split-GFP tagged CVB3 as a new tool for the direct visualization of enterovirus ROs in living cells, which will allow the study of their dynamics. Furthermore, the combination of live-cell imaging with CLEM will enable us to establish a direct link between events observed by fluorescence microscopy and morphologically distinct ROs, which could shed light onto the possible differentiated roles of these different virus-induced structures in enterovirus infection. This system will therefore serve as a valuable tool for future studies on the origin and function of enterovirus ROs.

FUNDING INFORMATION

This work was supported by research grants from the Netherlands Organisation for Scientific Research (NWO-VENI-863.12.005 to HMvdS, NWO-VENI-722.012.066 to JRPMS, NWO-VICI-91812628 to FJMvK, NWO-MEERVOUD 863.10.003 to MB) and the European Union 7th Framework (EUVIRNA Marie Curie Initial Training Network, grant agreement number 264286 to FJMvK). The funders had no role in study design, data collection and interpretation, or the decision to submit the work for publication.

ACKNOWLEDGEMENTS

The authors thank the staff at the LUMC light microscopy facility their technical help.

EXPERIMENTAL PROCEDURES

Cells. HeLa R19, BGM (buffalo green monkey), and COS-1 cells were grown in Dulbecco's minimal essential medium (DMEM, Lonza) supplemented with 10% fetal bovine serum and penicillin and streptomycin at 37oC and 5% CO2.

Plasmids and infectious clones. The expression construct encoding wild-type (wt) 3A, i.e. p3A-myc, was described elsewhere (64). GFP(S11), i.e. the residues RDHMVLHEYVNAAGIT, were inserted after amino acid 2 in CVB3 3A to yield p3A(S11aa2)-myc. For this, a forward primer containing the GFP(S11)-tag was used in a PCR reaction with p3A-myc as a template to generate 3A(S11aa2) as a PCR product. Wt 3A in p3A-myc was replaced with this PCR product using standard DNA cloning techniques. The same strategy was used to introduce GFP(S11) or the StrepII-tag (i.e. residues SAWSHPQFEK) in the infectious clone of CVB3 (p53CB3/T7) described elsewhere (64), yielding p53CB3-3A(S11aa2)/T7 or p53CB3-3A(StrepIIaa2)/T7. The GFP(S1-10) expression construct pCMV-mGFP(S1-10) was purchased from Sandia Biotech. For the production of CVB3 encoding both GFP(S1-10) and 3A(S11aa2), the GFP(S1-10) gene followed by a 3CD cleavage site was placed directly upstream of the capsid coding region P1 in p53CB3-3A(S11aa2)/T7, similar to modifications previously described for CVB3 encoding luciferase (27). For the production of MLVs (Murine Leukemia Virus particles), our genes of interest were cloned into the retroviral vectors pQCXIP (for GFP(S1-10) or mCherry-P4M-SidM) or pRetroQ-mCherry (for GM130), both purchased from Clontech, with standard DNA cloning techniques. In the resulting plasmids, the gene of interest is followed by an IRES and a puromycin resistance gene for the production of stable cell lines.

Retroviral particles and the production of stable cell lines. For the delivery of genes (i.e. GFP(S1-10), mCherry-GM130, or mCherry-SidM-P4M) into cells, we used an MLV-based retroviral vector system (Clontech). MLV stocks were produced by co-transfecting HEK293T cells with the plasmid pCAGGS-VSV-G encoding vesicular stomatitis virus protein G (VSV-G), the plasmid pMLV-Gag/Pol encoding the capsid proteins, reverse transcriptase, and integrase proteins, and the plasmid pQCXIP or pRetroQ-mCherry containing the gene of interest. Four to five days post-transfection, supernatants were harvested and cleared of cell debris by centrifugation and filtration through a 0.45 µm pore size filter. Stocks were buffered with 10 mM HEPES, aliquoted, and frozen at −80°C for later use. Prior to transduction, the MLV particles were 5 to 10 times concentrated

using a 100 kD-concentrator (Millipore). For the generation of single-cell clones stably expressing GFP(S1-10), BGM and HeLa cells were transduced and grown in the presence of puromycin (2 µg/ml for HeLa; 30 µg/ml for BGM) to generate pools of GFP(S1-10)-expressing cells, which were subsequently used to prepare single-cell clones by limiting dilution. Expression of GFP(S1-10) was monitored during passaging by immunofluorescence microscopy using the GFP antibody.

Mammalian two-hybrid assay. pACT, pBIND, and pG5Luc vectors were from Promega. pBIND-GBF1 encoding the N-terminus of GBF1, pACT-3A, and pBIND-3A were described previously (38, 39). pACT-ACBD3 was a kind gift from dr. J. Sasaki (Fujita Health University School of Medicine, Aichi, Japan) (45). pACT-3A(S11aa2) and pBIND-3A(S11aa2) were cloned with a forward primer containing the GFP(S11)-tag using standard DNA cloning techniques. Subconfluent layers of COS-1 cells seeded in 24 well plates were transfected with 350 ng of pACT, pBIND, and pG5Luc plasmids using Fugene6 (Promega) according to the manufacturer's protocol. At 48 h post-transfection (p.t.) cells were lysed and Renilla and Firefly luciferase levels were measured using the Dual-Luciferase assay kit (Promega) following the manufacturer's protocol. Values were converted to Firefly/Renilla signal ratios to correct for transfection efficiencies.

Virus infection. The production of CVB3 from infectious clones was described previously (39). Virus titers were determined by endpoint titration according to the method of Reed and Muench and expressed as 50% cell culture infective doses (CCID50). BGM or HeLa cells were infected with virus for 30 min to 1 hour. Following removal of the inoculum, fresh medium was added to the cells. At indicated time points, cells were either fixed for immunolabeling, lysed to measure the amount of viral RNA by quantitative PCR, or frozen to determine the amount of infectious virus particles by titration analysis.

Quantitative PCR. RNA was isolated from infected cells using a Nucleospin RNA kit (Machery-Nagel). cDNA was synthesized using random hexamers as primers with a TaqMan reverse transcription reagents kit (Roche). The cDNA was used for quantitative PCR with the forward primer 5'-CGTGGGGCTACAATCAAGTT-3', the reverse primer 5'-TAACAGGAGCTTTGGGCATC-3', and the LightCycler 480 SYBR Green I master kit (Roche) for 45 cycles (5 s at 95°C, 10 s at 60°C, and 20 s at 72°C) on a LightCycler 480 (Roche).

Western Blot analysis. Proteins were separated with 10% gradient PAGE using the Gradi-Gel™ gradient analysis kit (Elpis biotech). Samples were transferred to nitrocellulose membranes (Bio-Rad). After cutting the membrane in two at the 15 kD band of the marker, one membrane (proteins larger than 15 kD) was incubated with primary antibodies against mouse monoclonal anti-βactin (Sigma) and rabbit polyclonal anti-GFP described previously (44), which also recognizes GFP(S1-10). The membrane with proteins smaller than 15 kD was incubated with rabbit polyclonal anti-3A described previously (44). Secondary antibodies included IRDye 680-conjugated goat anti-mouse or IRDye 800-conjugated goat anti-rabbit (LI-COR). Images of blots were acquired with Odyssey Imaging System LI-COR.

Immunofluorescence microscopy. BGM or HeLa cells were grown to subconfluency on coverslips in 24-well plates. Where indicated, cells were transfected with 200 ng of plasmid DNA using Fugene6 according to the manufacturer's protocol or infected with CVB3-3A(S11aa2) at an MOI of 1-10. At 24 h p.t. or 5-6 h post-infection (p.i.), cells were fixed with 4% paraformaldehyde for 20 min at room temperature, followed by permeabilization with PBS-0.1% Triton X-100 for 10 min. Cells were then incubated sequentially with primary and secondary antibodies diluted in PBS containing

2% normal goat serum. Cellular proteins were detected with primary antibodies against PI4KIIIB (Millipore), GBF1 (BD Biosciences), COP-I (provided by F. Wieland, Biochemie-Zentrum, Heidelberg, Germany). GFP(S1-10) was detected with a GFP antibody and CVB3 3A proteins with a 3A antibody, both described previously (44). Conjugated goat anti-rabbit and goat anti-mouse Alexa Fluor 488 or Alexa Fluor 594 (Molecular Probes) were used as secondary antibodies. Nuclei were stained using DAPI. Coverslips were mounted with FluorSave (Calbiochem). Images were acquired with an Olympus BX60 fluorescence microscope with a 40x (0.75 NA) dry objective or a Leica SPE-II DMI-4000 confocal laser scanning microscope equipped with a 100x (1.4 NA) oil immersion objective, and the confocal pinhole adjusted to 1 airy unit (AU).

Live-cell imaging. BGM(GFPS1-10) cells were seeded in glass-bottom 4-chamber 35-mm dishes (CELLviewTM) and grown to ~35% confluency before transduction with MLV mCherry-GM130 particles. Infection with CVB3-3A(S11aa2) was carried out 18-24 hours later. Cells were washed with Fluorobrite medium (Thermo Fisher Scientific) supplemented with 8% fetal calf serum (FCS) and 25 mM HEPES just prior to imaging. Imaging was performed with a Leica SP5 confocal microscope equipped with a HyD detector and a 63x (1.4 NA) oil immersion objective, and the confocal pinhole adjusted to 95.56 µm as standard, or 600 µm to approximate wide-field imaging. Cells were maintained in a live-cell imaging chamber at 37°C and 5% CO2. GFP and mCherry were excited using a 488 nm or 561 nm laser respectively and appropriate emission filters, and positions (xyz) were marked and imaged sequentially at 5 minute intervals. For the generation of movies, live-cell imaging data were processed in ImageJ and aligned using the StackReg plugin.

Correlative light electron microscopy. Asymmetrical guide marks were scratched into glass-bottom 8-well chamber µ-slides (Ibidi), upon which BGM(GFPS1-10) cells were grown to subconfluency and infected with CVB3-3A(S11aa2). Just prior to imaging, and to later aid in the correlation of fluorescent and EM images, cells were incubated with 100 nM Mitotracker® Deep Red FM for 30 minutes, then washed several times in Fluorobrite medium supplemented with 8% FCS and 25 mM HEPES. Imaging was carried out from ~2 hours p.i. with a Leica SP8 confocal microscope equipped with a HyD detector, in a live-cell chamber at 37°C and 5% CO2 and using a 63x (1.4 NA) oil immersion objective. For each position of interest, a low resolution tile-scan was taken of the surrounding area, including guide marks, to aid in later re-identification. Z-stacks were acquired using a 1 AU pinhole and Nyquist frequency sampling. Cells were then fixed with 4% paraformaldehyde and 2.5% glutaraldehyde in 0.1 M Sørenson's phosphate buffer (PB) and processed for electron microscopy. Post-fixation was carried out with 1% osmium tetroxide for 1 hour in PB then 1% tannic acid in PB for 30 minutes, after which cells were serially dehydrated in ethanol and infiltrated and embedded in LX 112 resin (Ladd Research Industries) before polymerisation at 60°C. Positions of interest imaged earlier were identified on the resin block surface through comparison with (horizontally flipped) tilescan images, appropriate block-faces were trimmed and serial thin sections cut and collected on copper slot grids covered with a carbon-coated formvar layer. After post-staining grids with lead citrate and uranyl acetate, image meshes spanning large areas of the grid were collected on an FEI Tecnai 20 FEG electron microscope operated at 120 kV with a 4k x4k pixel charge-couple device (CCD) camera (US4000, Gatan) with binning 2 and a final image pixel size of 1.94nm. These individual images were later combined into composite stitches (65). Cells of interest were digitally extracted from their raw image files using ImageJ and Aperio Imagescope software packages for light microscope and electron microscope images, respectively. These

images were then overlaid using Adobe Photoshop CS6. The mitochondrial pattern in the EM images was compared with the Mitotracker® Deep Red FM signal to find the right transformations to correlate both types of data. While the discrepancy in the axial resolution of light and electron microscopes limited the precision of the overlay, the use of this secondary marker was critical to determine the z-plane in the confocal data the best fit the EM cell section under analysis and for xy orientation of both images, thus providing an independent marker for an unbiased localization of the 3A signal.

REFERENCES

1. Tapparel C, Siegrist F, Petty TJ, Kaiser L. 2013. Picornavirus and enterovirus diversity with associated human diseases. Infect. Genet. Evol. 14:282–93.
2. den Boon JA, Ahlquist P. 2010. Organelle-like membrane compartmentalization of positive-strand RNA virus replication factories. Annu. Rev. Microbiol. 64:241–56.
3. Miller S, Krijnse-Locker J. 2008. Modification of intracellular membrane structures for virus replication. Nat. Rev. Microbiol. 6:363–74.
4. Romero-Brey I, Bartenschlager R. 2014. Membranous replication factories induced by plus-strand RNA viruses. Viruses 6:2826–57.
5. Belov GA, van Kuppeveld FJM. 2012. (+)RNA viruses rewire cellular pathways to build replication organelles. Curr. Opin. Virol. 2:740–7.
6. van der Linden L, Wolthers KC, van Kuppeveld FJM. 2015. Replication and Inhibitors of Enteroviruses and Parechoviruses. Viruses 7:4529–62.
7. Neufeldt CJ, Joyce MA, Van Buuren N, Levin A, Kirkegaard K, Gale M, Tyrrell DLJ, Wozniak RW. 2016. The Hepatitis C Virus-Induced Membranous Web and Associated Nuclear Transport Machinery Limit Access of Pattern Recognition Receptors to Viral Replication Sites. PLoS Pathog. 12:e1005428.
8. Overby AK, Popov VL, Niedrig M, Weber F. 2010. Tick-borne encephalitis virus delays interferon induction and hides its double-stranded RNA in intracellular membrane vesicles. J. Virol. 84:8470–83.
9. Bienz K, Egger D, Rasser Y, Bossart W. 1983. Intracellular distribution of poliovirus proteins and the induction of virus-specific cytoplasmic structures. Virology 131:39–48.
10. Bienz K, Egger D, Pasamontes L. 1987. Association of polioviral proteins of the P2 genomic region with the viral replication complex and virus-induced membrane synthesis as visualized by electron microscopic immunocytochemistry and autoradiography. Virology 160:220–6.
11. Wong J, Zhang J, Si X, Gao G, Mao I, McManus BM, Luo H. 2008. Autophagosome supports coxsackievirus B3 replication in host cells. J. Virol. 82:9143–9153.
12. Schlegel A, Giddings TH, Ladinsky MS, Kirkegaard K. 1996. Cellular origin and ultrastructure of membranes induced during poliovirus infection. J. Virol. 70:6576–88.
13. Suhy DA, Giddings TH, Kirkegaard K. 2000. Remodeling the endoplasmic reticulum by poliovirus infection and by individual viral proteins: an autophagy-like origin for virus-

induced vesicles. J. Virol. 74:8953–65.
14. Kemball CC, Alirezaei M, Flynn CT, Wood MR, Harkins S, Kiosses WB, Whitton JL. 2010. Coxsackievirus infection induces autophagy-like vesicles and megaphagosomes in pancreatic acinar cells in vivo. J. Virol. 84:12110–24.
15. Volle R, Archimbaud C, Couraud P-O, Romero IA, Weksler B, Mirand A, Pereira B, Henquell C, Peigue-Lafeuille H, Bailly J-L. 2015. Differential permissivity of human cerebrovascular endothelial cells to enterovirus infection and specificities of serotype EV-A71 in crossing an in vitro model of the human blood-brain barrier. J. Gen. Virol. 96:1682–95.
16. Alirezaei M, Flynn CT, Wood MR, Harkins S, Whitton JL. 2015. Coxsackievirus can exploit LC3 in both autophagy-dependent and -independent manners in vivo. Autophagy 11:1389–407.
17. Belov GA, Nair V, Hansen BT, Hoyt FH, Fischer ER, Ehrenfeld E. 2012. Complex dynamic development of poliovirus membranous replication complexes. J. Virol. 86:302–12.
18. Limpens RWAL, van der Schaar HM, Kumar D, Koster AJ, Snijder EJ, van Kuppeveld FJM, Bárcena M. 2011. The transformation of enterovirus replication structures: a three-dimensional study of single- and double-membrane compartments. MBio 2.
19. Jackson WT, Giddings TH, Taylor MP, Mulinyawe S, Rabinovitch M, Kopito RR, Kirkegaard K. 2005. Subversion of Cellular Autophagosomal Machinery by RNA Viruses. PLoS Biol. 3:e156.
20. Chen Y-H, Du W, Hagemeijer MC, Takvorian PM, Pau C, Cali A, Brantner CA, Stempinski ES, Connelly PS, Ma H-C, Jiang P, Wimmer E, Altan-Bonnet G, Altan-Bonnet N. 2015. Phosphatidylserine vesicles enable efficient en bloc transmission of enteroviruses. Cell 160:619–30.
21. Bird SW, Maynard ND, Covert MW, Kirkegaard K. 2014. Nonlytic viral spread enhanced by autophagy components. Proc. Natl. Acad. Sci. U. S. A. 111:13081–6.
22. Hsu N-Y, Ilnytska O, Belov G, Santiana M, Chen Y-H, Takvorian PM, Pau C, van der Schaar H, Kaushik-Basu N, Balla T, Cameron CE, Ehrenfeld E, van Kuppeveld FJM, Altan-Bonnet N. 2010. Viral reorganization of the secretory pathway generates distinct organelles for RNA replication. Cell 141:799–811.
23. Belov GA, Altan-Bonnet N, Kovtunovych G, Jackson CL, Lippincott-Schwartz J, Ehrenfeld E. 2007. Hijacking components of the cellular secretory pathway for replication of poliovirus RNA. J. Virol. 81:558–67.
24. Richards AL, Soares-Martins JAP, Riddell GT, Jackson WT. 2014. Generation of unique poliovirus RNA replication organelles. MBio 5:e00833–13.
25. Rust RC, Landmann L, Gosert R, Tang BL, Hong W, Hauri HP, Egger D, Bienz K. 2001. Cellular COPII proteins are involved in production of the vesicles that form the poliovirus replication complex. J. Virol. 75:9808–9818.
26. Schnell U, Dijk F, Sjollema KA, Giepmans BNG. 2012. Immunolabeling artifacts and the need for live-cell imaging. Nat. Methods 9:152–8.
27. Lanke KHW, van der Schaar HM, Belov G a, Feng Q, Duijsings D, Jackson CL, Ehrenfeld E, van Kuppeveld FJM. 2009. GBF1, a guanine nucleotide exchange factor for Arf, is crucial for coxsackievirus B3 RNA replication. J. Virol. 83:11940–9.
28. Shang B, Deng C, Ye H, Xu W, Yuan Z, Shi P-Y, Zhang B. 2013. Development and characterization of a stable eGFP enterovirus 71 for antiviral screening. Antiviral Res. 97:198–205.

29. Robinson SM, Tsueng G, Sin J, Mangale V, Rahawi S, McIntyre LL, Williams W, Kha N, Cruz C, Hancock BM, Nguyen DP, Sayen MR, Hilton BJ, Doran KS, Segall AM, Wolkowicz R, Cornell CT, Whitton JL, Gottlieb RA, Feuer R. 2014. Coxsackievirus B Exits the Host Cell in Shed Microvesicles Displaying Autophagosomal Markers. PLoS Pathog. 10:e1004045.
30. Belov G a, Feng Q, Nikovics K, Jackson CL, Ehrenfeld E. 2008. A critical role of a cellular membrane traffic protein in poliovirus RNA replication. PLoS Pathog. 4:e1000216.
31. Teterina NL, Levenson EA, Ehrenfeld E. 2010. Viable polioviruses that encode 2A proteins with fluorescent protein tags. J. Virol. 84:1477–88.
32. Teterina NL, Pinto Y, Weaver JD, Jensen KS, Ehrenfeld E. 2011. Analysis of poliovirus protein 3A interactions with viral and cellular proteins in infected cells. J. Virol. 85:4284–96.
33. de Jong AS, Melchers WJG, Glaudemans DHRF, Willems PHGM, van Kuppeveld FJM. 2004. Mutational analysis of different regions in the coxsackievirus 2B protein: requirements for homo-multimerization, membrane permeabilization, subcellular localization, and virus replication. J. Biol. Chem. 279:19924–35.
34. Cabantous S, Terwilliger TC, Waldo GS. 2005. Protein tagging and detection with engineered self-assembling fragments of green fluorescent protein. Nat. Biotechnol. 23:102–107.
35. Towner JS, Ho T V, Semler BL. 1996. Determinants of membrane association for poliovirus protein 3AB. J. Biol. Chem. 271:26810–8.
36. Pédelacq J-D, Cabantous S, Tran T, Terwilliger TC, Waldo GS. 2006. Engineering and characterization of a superfolder green fluorescent protein. Nat. Biotechnol. 24:79–88.
37. Teterina NL, Lauber C, Jensen KS, Levenson EA, Gorbalenya AE, Ehrenfeld E. 2011. Identification of tolerated insertion sites in poliovirus non-structural proteins. Virology 409:1–11.
38. Dorobantu CM, Ford-Siltz LA, Sittig SP, Lanke KHW, Belov GA, van Kuppeveld FJM, van der Schaar HM. 2015. GBF1- and ACBD3-Independent Recruitment of PI4KIIIB to Replication Sites by Rhinovirus 3A Proteins. J. Virol. 89:1913–1918.
39. Dorobantu CM, van der Schaar HM, Ford LA, Strating JRPM, Ulferts R, Fang Y, Belov G, van Kuppeveld FJM. 2013. Recruitment of PI4KIIIB to coxsackievirus B3 replication organelles is independent of ACBD3, GBF1, and Arf1. J. Virol.
40. Lee MCS, Miller EA, Goldberg J, Orci L, Schekman R. 2004. Bi-directional protein transport between the ER and Golgi. Annu. Rev. Cell Dev. Biol. 20:87–123.
41. Bonifacino JS, Glick BS. 2004. The mechanisms of vesicle budding and fusion. Cell 116:153–66.
42. Cornell CT, Kiosses WB, Harkins S, Whitton JL. 2006. Inhibition of protein trafficking by coxsackievirus b3: multiple viral proteins target a single organelle. J. Virol. 80:6637–47.
43. Doedens JR, Kirkegaard K. 1995. Inhibition of cellular protein secretion by poliovirus proteins 2B and 3A. EMBO J. 14:894–907.
44. Wessels E, Duijsings D, Niu T-K, Neumann S, Oorschot VM, de Lange F, Lanke KHW, Klumperman J, Henke A, Jackson CL, Melchers WJG, van Kuppeveld FJM. 2006. A viral protein that blocks Arf1-mediated COP-I assembly by inhibiting the guanine nucleotide exchange factor GBF1. Dev. Cell 11:191–201.
45. Sasaki J, Ishikawa K, Arita M, Taniguchi K. 2012. ACBD3-mediated recruitment of PI4KB to picornavirus RNA replication sites. EMBO J. 31:754–66.

46. Greninger AL, Knudsen GM, Betegon M, Burlingame AL, Derisi JL. 2012. The 3A protein from multiple picornaviruses utilizes the golgi adaptor protein ACBD3 to recruit PI4KIIIβJ. Virol. 86:3605–16.
47. Téoulé F, Brisac C, Pelletier I, Vidalain P-O, Jégouic S, Mirabelli C, Bessaud M, Combelas N, Autret A, Tangy F, Delpeyroux F, Blondel B. 2013. The Golgi protein ACBD3, an interactor for poliovirus protein 3A, modulates poliovirus replication. J. Virol.
48. Langereis MA, Rabouw HH, Holwerda M, Visser LJ, van Kuppeveld FJM. 2015. Knockout of cGAS and STING Rescues Virus Infection of Plasmid DNA-Transfected Cells. J. Virol. 89:11169–73.
49. de Boer P, Hoogenboom JP, Giepmans BNG. 2015. Correlated light and electron microscopy: ultrastructure lights up! Nat. Methods 12:503–13.
50. Gibson KH, Vorkel D, Meissner J, Verbavatz J-M. 2014. Fluorescing the electron: strategies in correlative experimental design. Methods Cell Biol. 124:23–54.
51. Mattion NM, Reilly PA, DiMichele SJ, Crowley JC, Weeks-Levy C. 1994. Attenuated poliovirus strain as a live vector: expression of regions of rotavirus outer capsid protein VP7 by using recombinant Sabin 3 viruses. J. Virol. 68:3925–33.
52. Brandenburg B, Zhuang X. 2007. Virus trafficking - learning from single-virus tracking. Nat. Rev. Microbiol. 5:197–208.
53. Wölk B, Büchele B, Moradpour D, Rice CM. 2008. A dynamic view of hepatitis C virus replication complexes. J. Virol. 82:10519–31.
54. Eyre NS, Fiches GN, Aloia AL, Helbig KJ, McCartney EM, McErlean CSP, Li K, Aggarwal A, Turville SG, Beard MR. 2014. Dynamic imaging of the hepatitis C virus NS5A protein during a productive infection. J. Virol. 88:3636–52.
55. Schramm B, de Haan CAM, Young J, Doglio L, Schleich S, Reese C, Popov A V, Steffen W, Schroer T, Locker JK. 2006. Vaccinia-virus-induced cellular contractility facilitates the subcellular localization of the viral replication sites. Traffic 7:1352–67.
56. Cotton S, Grangeon R, Thivierge K, Mathieu I, Ide C, Wei T, Wang A, Laliberté J-F. 2009. Turnip mosaic virus RNA replication complex vesicles are mobile, align with microfilaments, and are each derived from a single viral genome. J. Virol. 83:10460–71.
57. Hagemeijer MC, Verheije MH, Ulasli M, Shaltiël IA, de Vries LA, Reggiori F, Rottier PJM, de Haan CAM. 2010. Dynamics of coronavirus replication-transcription complexes. J. Virol. 84:2134–49.
58. Hagemeijer MC, Ulasli M, Vonk AM, Reggiori F, Rottier PJM, de Haan CAM. 2011. Mobility and interactions of coronavirus nonstructural protein 4. J. Virol. 85:4572–7.
59. van den Born E, Posthuma CC, Knoops K, Snijder EJ. 2007. An infectious recombinant equine arteritis virus expressing green fluorescent protein from its replicase gene. J. Gen. Virol. 88:1196–205.
60. Griffin BA, Adams SR, Tsien RY. 1998. Specific covalent labeling of recombinant protein molecules inside live cells. Science 281:269–72.
61. Adams SR, Campbell RE, Gross LA, Martin BR, Walkup GK, Yao Y, Llopis J, Tsien RY. 2002. New biarsenical ligands and tetracysteine motifs for protein labeling in vitro and in vivo: synthesis and biological applications. J. Am. Chem. Soc. 124:6063–76.
62. Avilov S V, Moisy D, Munier S, Schraidt O, Naffakh N, Cusack S. 2012. Replication-competent

influenza A virus that encodes a split-green fluorescent protein-tagged PB2 polymerase subunit allows live-cell imaging of the virus life cycle. J. Virol. 86:1433–48.

63. Drummond CG, Nickerson CA, Coyne CB. 2016. A Three-Dimensional Cell Culture Model To Study Enterovirus Infection of Polarized Intestinal Epithelial Cells. mSphere 1:e00030–15.

64. Wessels E, Duijsings D, Notebaart RA, Melchers WJG, van Kuppeveld FJM. 2005. A proline-rich region in the coxsackievirus 3A protein is required for the protein to inhibit endoplasmic reticulum-to-golgi transport. J. Virol. 79:5163–73.

65. Faas FGA, Avramut MC, van den Berg BM, Mommaas AM, Koster AJ, Ravelli RBG. 2012. Virtual nanoscopy: generation of ultra-large high resolution electron microscopy maps. J. Cell Biol. 198:457–69.

SUPPLEMENTAL FIGURES

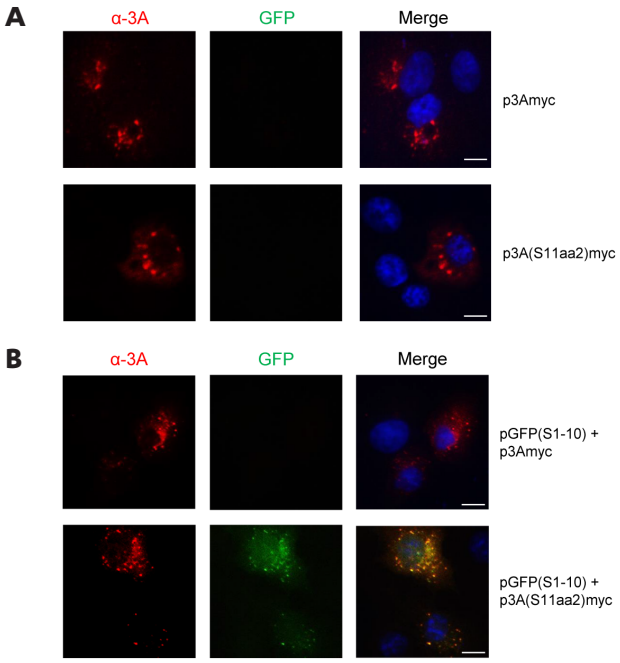

Figure S1. Co-expression of 3A(S11aa2) with GFP(S1-10) yields GFP fluorescence. A) Introduction of GFP(S11) into 3A does not alter its expression pattern. HeLa cells were transfected with plasmids encoding wild-type (wt) 3A (p3A-myc) or tagged 3A (p3A(S11aa2)-myc). One day later, the 3A protein was stained with an antibody directed against 3A and a secondary Alexa594-labeled antibody. B) GFP fluorescence is only detected when GFP(S1-10) is co-expressed with 3A(S11aa2). BGM cells were co-transfected with the plasmid encoding GFP(S1-10) (pGFP(S1-10)) and either p3A-myc or p3A(S11aa2)-myc. One day later, the 3A protein was stained with a primary antibody directed against 3A and a secondary Alexa594-labeled antibody. A, B) Nuclei were stained with DAPI. Wide-field images were acquired with an Olympus BX60 fluorescence microscope. Scale bars equal 10 µm.

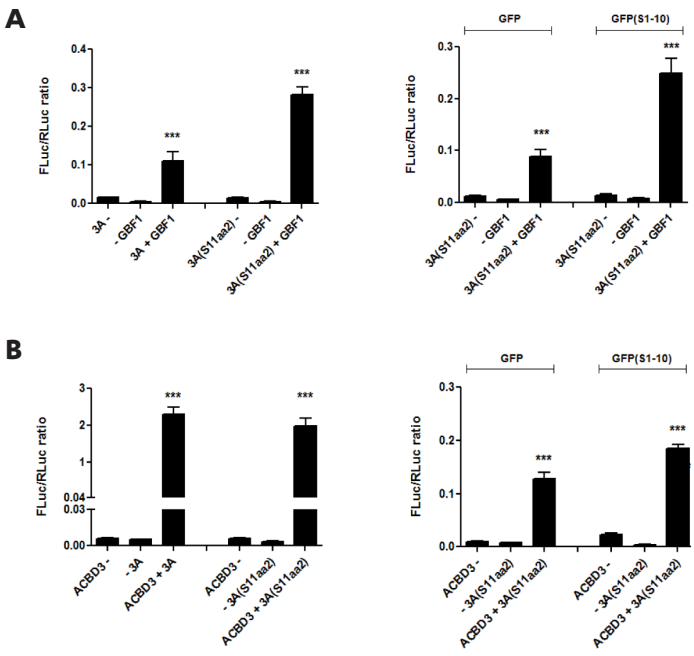

Figure S2. 3A(S11aa2) interacts with host factors GBF1 and ACBD3. A, B) A mammalian two-hybrid assay was used to determine the ability of 3A(S11aa2) to interact with the N-terminus of GBF1 (A) or ACBD3 (B). This assay was conducted in the absence of GFP(S1-10) (left graphs) or in the presence of GFP(S1-10) (right graphs) using full-length GFP as a transfection control. Bars represent the means of three samples ± standard deviations. Significant differences were calculated over the highest control sample by a paired Student t-test. ***, P<0.001

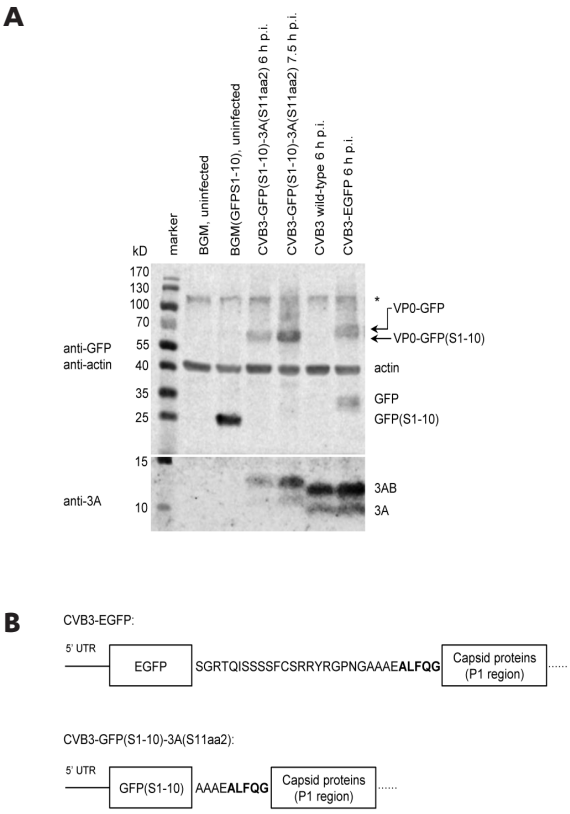

Figure S3. Processing of the artificial 3CD cleavage site between a foreign protein and P1 is suboptimal. A) BGM cells were infected with different CVB3 and lysates were prepared at the indicated time points. Cell lysates were subjected to Western Blot analysis using antibodies against actin (loading control), 3A (infection control), or GFP that also recognizes GFP(S1-10). An aspecific band is indicated with an asterisk. BGM cells that stably express GFP(S1-10) showed a band at around 25 kD, which is in accordance with the somewhat smaller size than full-length GFP (27 kD). BGM cells infected with CVB3-GFP(S1-10)-3A(S11aa2) accumulated a clear band at around 60 kD, which corresponds to the precursor VP0 (36 kD) fused to GFP(S1-10). Little, if any, GFP(S1-10) was detectable, indicating a defect in processing. We also examined CVB3-EGFP (27), which also is delayed in replication compared to wild-type CVB3, but not as severely as CVB3-GFP(S1-10)-3A(S11aa2). In these samples, GFP is detected as a fusion protein to VP0 as well as an individual protein. Both results demonstrate that processing of the artificial 3CD cleavage site is suboptimal. Why cleavage of full-length GFP from VP0 appeared more efficient than for CVB3-GFP(S1-10)-3A(S11aa2) remains to be determined. Since GFP(S1-10) folds differently than full-length EGFP, this may affect processing of the cleavage site. Also, EGFP is followed by a longer linker sequence upstream of the cleavage site (ALFQG, indicated in bold) compared to GFP(S1-10) (shown in B) due to cloning procedures, which may affect protein folding and processing.

Movie S1. Golgi disruption and 3A accumulation monitored over the course of CVB3 infection. Cropped view showing Golgi fragmentation at higher resolution (images are of cell shown in Figure 8B) from ~2 to 7.5 hours post infection. Fragmentation can be observed from approximately 3.5 hours post infection, and complete disassembly occurs within 30 minutes as evidenced by the punctate GM130 signal. Scale bar equals 10 µm, frame rate is 4 fps. Images were collected at 5 minute intervals.

Movie S2. The split-GFP system allows 3A to be monitored over the full course of CVB3 infection. Overview of a typical field of view during live-cell experiments from ~5 to 10 hours post infection (shown first with green, red and brightfield channels, then repeated with green and red channels only). Several phases of infection can be observed, including the developing 3A-GFP signal and associated disruption of Golgi morphology, and the accumulation of ROs in the cytoplasm leading ultimately to cell lysis. Scale bar equals 10 µm, frame rate is 4 fps. Images were collected at 5 minute intervals.